Soft Matter

Dynamic Article Links

Cite this: *Soft Matter*, 2011, **7**, 4644

www.rsc.org/softmatter

PAPER

Hair cell inspired mechanotransduction with a gel-supported, artificial lipid membrane

Stephen A. Sarles,[a] John D. W. Madden[b] and Donald J. Leo*[a]

Received 24th January 2011, Accepted 21st March 2011
DOI: 10.1039/c1sm05120b

A gel-supported lipid bilayer formed at the base of an artificial hair is used as the transduction element in an artificial, membrane-based hair cell sensor inspired by the structure and function of mammalian hair cells. This paper describes the initial fabrication and characterization of a bioderived, soft-material alternative to previous artificial hair cells that used the transduction properties of synthetic materials for flow and touch sensing. Under an applied air flow, the artificial hair structure vibrates, triggering a picoamp-level electrical current across the lipid bilayer. Experimental analysis of this mechanoelectrical transduction process supports the hypothesis that the current is produced by a time-varying change in the capacitance of the membrane caused by the vibration of the hair. Specifically, frequency analysis of both the motion of the hair and the measured current show that both phenomena occur at similar frequencies (0.1–1.0 kHz), which suggests that changes in capacitance occur as a result of membrane bending during excitation. In this paper, the bilayer-based hair cell sensor is experimentally characterized to understand the effects of transmembrane potential, the applied air flow, and the dimensions of the hair.

1 Introduction

Sensory hairs, or hair cells, are common in many animal species, including fish,[1,2] insects,[3,4] and mammals,[5,6] where the diversity found in the design of the hair cell enables the detection of a wide range of stimuli, including: sound, flow, vibration, and even inertial tilt. The diversity of stimuli-responsive behavior of natural hair cells provides inspiration for developing engineered systems that also perform mechanoelectrical transduction for a variety of sensing applications.

In recent years several embodiments of hair cell sensors have been developed that use the electromechanical properties of synthetic materials to produce an electrical response as a result of the bending of an artificial hair. Most notably, Liu's research group pioneered several generations of artificial cilia for flow and touch sensing. Their first iteration of a hair cell array used a polyurethane force sensitive resistor at the base of each polymeric hair to produce changes in voltage in a bridge circuit as a result of bending of the hair.[7] The second generation demonstrated the use of magnetic assembly to orient polyimide composite cilia.[8] A strain gauge positioned at the base of these structures converted the mechanical bending of the cilia into an electrical signal. The third generation, inspired by the hair cell structures found along the lateral lines of fish, utilized piezoresistive cilia encapsulated by a cupola-shaped hydrogel. This bio-inspired design demonstrated that the gel encapsulation reduces the background noise, thereby improving the detection limit at low flow rates and increasing the dynamic range of the sensor.[9,10] In other approaches, magnetostrictive materials such as Galfenol (an iron-gallium alloy) have been used to fabricate mm- and nm-scale cilia arrays that produce a mechano-magnetic response to dynamic bending.[11–14]

One of the primary differences between the aforementioned embodiments of artificial hair cells and natural hair cells is the mechanism for mechanoelectric transduction. Cellular structures in hair cells use the same soft materials found in nearly all cells, namely phospholipids and proteins, as the primary transduction element. In particular, auditory hair cells of mammals rely heavily on soft membrane structures to generate and use polarization, mediate controlled transport through strain-activated ion channels, and provide compartmentalization for the cell.[5,6,15] Even the stereocilia of hair cells, which are used in the initial transduction process, are structural filaments encased within cell membranes.[16] Membranes in outer hair cells (OHCs) also contribute directly to *electromotility*, a process by which the electromechanical properties of the cell membranes that make up the lateral wall allow the cell to rapidly change shape in response to a change in polarization.[5,6,15] Thus, OHCs function in concert with inner hair cells (IHCs) to form a neural feedback loop that produces an adjustable mechanical amplification, where tunable gain enables both the detection of extremely low noise levels

[a]*Center for Intelligent Material Systems and Structures (CIMSS), Department of Mechanical Engineering, Virginia Tech, Blacksburg, VA, 24061, USA. E-mail: donleo@vt.edu; Fax: +1 (540) 231 2903; Tel: +1 (540) 231-2906*

[b]*Advanced Materials & Process Engineering Lab, Department of Electrical & Computer Engineering, University of British Columbia, Vancouver, B.C., V6T 1Z4, Canada*

(*i.e.* thermal noise) and a wide range of frequencies (from few hertz to nearly 70 kHz[5,15]).

While much is still being learned as to how these cells translate polarization of the inner cell volume into a mechanical strain (*i.e.* is the membrane stretched or is it bent?), it is generally accepted that prestin proteins in the plasma membrane function as molecular motors that move charge across the membrane in order to produce motion.[16,17] Recent analysis by Sachs, *et al.* specifically suggests that the prestin molecules generate motion by using polarization to induce local changes in the curvature of the membrane.[15] This phenomenon is called the flexoelectric effect[18–21] as it relates the polarization of a material to the mechanical strain gradient. And in liquid crystals, including artificial lipid bilayers, direct flexoelectricity (FE) enables the development of a curvature-induced polarization (sensing),[20] while the converse FE effect is a polarization-induced curvature (actuation).[19]

Inspired by the multiple roles of membrane structures in mammalian hearing, we present a new type of hair cell sensor in which the mechanoelectrical properties of a 5 nm-thick artificial cell membrane provide the transduction mechanism for sensing air flow. This work builds on recent advances in the development of durable, encapsulated interface bilayers that are formed at the interface between lipid-encased aqueous volumes contained in a flexible substrate.[22–24] A unique feature of our approach is the ability to form a lipid bilayer on the surface of a lipid-encased gel that also supports an artificial hair.[24] Specifically, an artificial cell membrane, or lipid bilayer, connects two aqueous media; with one being a water-swollen, lipid-encased hydrogel volume used to support an artificial cilia and the second, a lipid-encased aqueous volume. Mechanical vibrations of the cilia caused by air flow translate motion to the gel and the lipid bilayer and generate a measurable current. The response of the hair cell due to air flow is characterized as a function of flow velocity, hair dimensions, and transmembrane potential and the physical mechanism for current generation is explained.

2 Materials and methods

2.1 Device description and fabrication

The hair cell inspired flow sensor presented in this paper builds on the work in our group to assemble and encapsulate artificial cell membranes within flexible substrates.[23,24] As shown in Fig. 1, a synthetic cilia-like structure rooted in a water-swollen polymeric gel is held vertically in one compartment of a flexible supporting substrate. A second, lipid-encased aqueous volume consisting of phospholipid vesicle solution contained in the adjacent compartment of the substrate connects to the hydrogel to form a lipid bilayer at the interface between the two compartments. Both compartments also contain an immiscible oil needed for promoting phospholipid self-assembly. The substrate used in this work is constructed from a transparent polyurethane (ClearFlex 50, Smooth-On, Inc.) and features the same geometry as a previous design used in first demonstrating bilayer formation within a flexible substrate.[23] The substrate serves to both support the assembly but also to regulate contact between the gel and the adjacent aqueous volume for bilayer formation through the application of mechanical force.

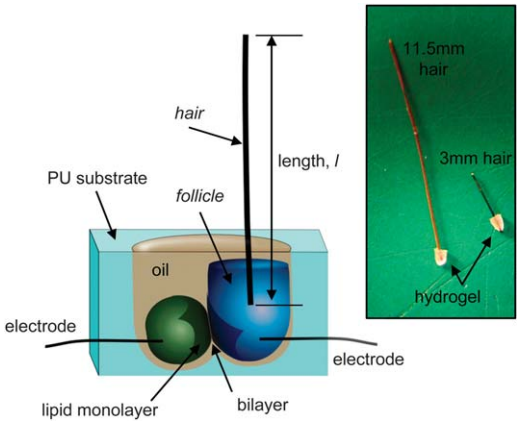

Fig. 1 The artificial hair cell characterized in this work consists of an artificial cell membrane (lipid bilayer) that connects two lipid-encased aqueous volumes, one being a liquid volume and the second being a water-swollen hydrogel that also features a synthetic hair. A lipid monolayer (shown artistically as a partial shell) fully encases each aqueous volume when submerged in oil.

The artificial hair cell consists of a *hair* fashioned from a commercially-available synthetic fiber and a *follicle* made from a volume of polymeric hydrogel as shown in the inset of Fig. 1. The average diameter of the fibers used in this work is 107 ± 19 μm ($n = 10$). The modulus of the fibers is measured to be 8.5 GPa and the density is measured to be 1.3 g cm^{-3}. The hydrogel follicle is made from a mixture of 40% (w/v) polyethylene glycol dimethacrylate (PEG-DMA, MW = 1000 g/mole, PolySciences, Inc.) and 0.25% (w/v) Irgacure 2959 (Ciba) photoinitiator in 500 mM potassium chloride (KCl, Sigma Aldrich), 10 mM 4-morpholinepropanesulfonic acid (MOPS, Sigma Aldrich), pH 7 buffer solution. The hydrogel is formed around the base of a suspended hair by photopolymerization in a separate polyurethane substrate.[24] After gel formation, the free end of the hair is trimmed to the desired length, l, and the hair cell (follicle with hair) is positioned in one compartment of the substrate. Prior to hair cell placement, both compartments of the substrate are filled with hexadecane (99%, Sigma). A small volume (~100 nl) of 2 mg mL^{-1} diphytanoyl phosphocholine (DPhPC) phospholipid vesicles (purchased as lyophilized powder, Avanti Polar Lipids, Inc.) suspended in 500 mM KCl (Sigma), 10 mM MOPS (Sigma), pH 7 buffer solution is then added to the same compartment in order to rehydrate the gel (which dehydrates slightly during curing) and provide phospholipids needed for monolayer assembly and bilayer formation. Finally, 200 nl of aqueous vesicle solution is pipetted into the vacant compartment.

Using the regulated attachment method,[23] the two aqueous phases are kept separated for approximately two minutes by compressing the substrate such that the aperture between the two compartments is closed sufficiently to prevent contact (a detailed discussion and illustrations of this technique can be found in our earlier work[23]). The aperture is reopened in order to allow the two lipid-encased volumes to come into contact, resulting in the formation of a lipid bilayer within a few seconds after initial contact. The RAM technique is also employed to control the areal size of the resulting bilayer—more compression of the

substrate produces less contact between the two volumes, while less compression allows for a larger bilayer to form.[23] Ultimately, the amount to which a lipid bilayer forms between opposing liquid-supported lipid monolayers will grow is a function of several parameters: the type of oil used,[25] the applied electrical potential,[26,27] and any physical constraints on the aqueous volumes that either inhibit or promote contact. The regulated attachment method controls this last parameter for prescribing bilayer formation and size. In this work, a 6.4 mm diameter aluminum rod mounted to the electrode holder of a motorized micromanipulator (SM325, WPI, Inc.) is used to incrementally compress the flexible substrate for controlling bilayer formation and size (Fig. 2a). Due to the soft nature of the hair cell system, we typically form a new hydrogel/hair/bilayer system for each set of tests.

The assembled hair cell system featuring an artificial membrane is subjected to a horizontal air flow that exits a 6.5 mm inner diameter tube positioned approximately 25 mm away from the hair location (Fig. 2b). Rather than the flow velocity, the exit pressure of a pressurized (>550 kPa) air source is controlled with a 0–35 kPa pressure regulator during measurements.

2.2 Electrical recordings and imaging

Silver–silver chloride (Ag/AgCl) electrodes made by chloriding 125 μm silver wire (Goodfellow) in household bleach are inserted through the sides of the substrate into each aqueous volume to enable electrical measurements of bilayer capacitance and air flow-induced current. The capacitance of the membrane is computed from the measured current induced by a triangular waveform voltage (10 mV, 20 Hz) as described elsewhere.[24] Sensing currents generated during the flow of air across the hair are measured with an AxoPatch 200B (Molecular Devices), which is also used to supply a dc potential across the membrane during each test. Measured currents are sampled at rate of 4 kHz and low-pass filtered at 2 kHz, respectively, before being converted to a digital signal with a DigiData 1440A (Molecular Devices) data acquisition system and recorded in AxoScope 10 software (Molecular Devices). Synchronized current measurements obtained during high speed video recording are sampled and filtered at 2 kHz and 1 kHz, respectively, in order to match the frame rate of the camera. All electrical recordings are performed within a Faraday cage for shielding.

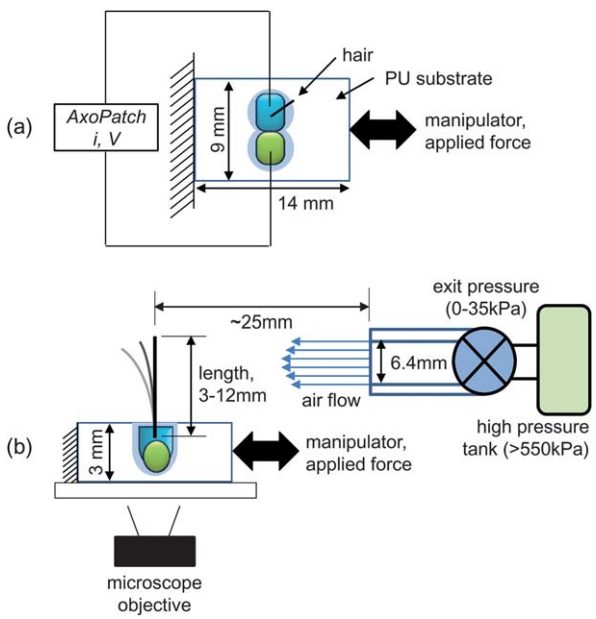

Fig. 2 (a) A top view of the experimental setup shows how a micromanipulator is used to applied forces to the substrate in order to control bilayer formation and size. Electrical recordings are made *via* electrodes that pierce through the substrate to make contact with each aqueous volume. (b) The corresponding side view shows how air flow is applied to the vertical hair structure held within the substrate. The substrate sits on the work stage of a microscope. Note: drawing is not to scale.

High speed video of the motion of the hair is captured at a frame rate of 2000 frames per second (fps) with a MotionScope PCI-2000S (RedLake) camera and a 25 mm TV lens and recorded in MotionScope software. A time vector of the position of the tip of the hair is then obtained by tracking specific pixels in the video using SAI Image Express Motion Trace software.

3 Results and discussion

3.1 Representative sensor response

The electrical response of the artificial hair cell sensor to an applied air flow is measured after forming a bilayer between the hydrogel base and the adjacent lipid-encased aqueous volume. Prior to membrane formation, the separated aqueous volumes are electrically isolated from one another and no current is measured between the electrodes. However, when the two aqueous phases connect to form a lipid bilayer, the capacitance of the interface increases as the two monolayers exclude excess solvent and form a thinned, two-molecule thick bilayer structure.[24,25] Measurements of capacitance verify this molecular (and electrical) change and provide information about when the bilayer has reached its final size. The capacitance of bilayers formed in this study ranged from 50–400 pF, corresponding to an equivalent diameter of the interface of 100–300 μm for a specific capacitance of 0.6 μF cm^{-2} for DPhPC bilayers.[28]

Fig. 3a shows a representative temporal response for the measured current through a bilayer when air, at a regulated exit pressure of 2.1 kPa (0.3 psi), flows across a 12 mm long hair used to form the hair cell sensor. Initially, the background current measured across the membrane is only a few picoamps when no flow is present and the hair is still. When air flow perturbs the hair ($4 < t < 14$ s), however, the hair vibrates and the amplitude of the measured current increases, yet the average value does not change. At the onset of air flow, we also observe that the current does not increase to the maximum amplitude instantaneously due to the time needed to manually adjust the pressure gage to the desired pressure level. The current then returns to its original amplitude when the flow is removed ($t \approx 15$ s). The root mean square amplitude of the current measured when no flow is present is approximately 1.97 pA (RMS) compared to 5.08 pA (RMS) when air is flowing across the hair.

In comparison, the flow of air across the same system that lacks a hair produces a much smaller change in measured current as is shown in Fig. 3b. Measurements at low flow pressures

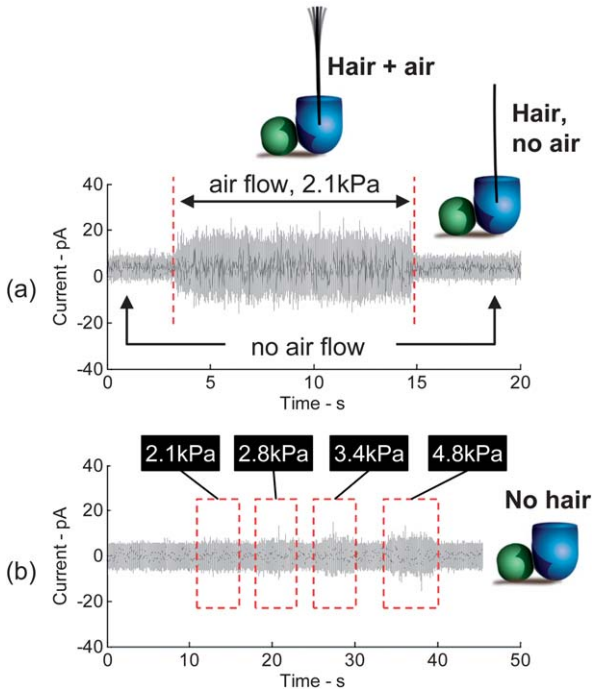

Fig. 3 (a) The measured current during air flow across a membrane-based hair cell sensor and (b) a control measurement of the current produced by the flow of air across the same bilayer system that does not have a hair.

(<2.1 kPa (0.3 psi)) do not produce an observable change in the measured current signal. At higher air flow pressures, the current response is greater than that of the current when no flow is present and is likely due to the open style design of the substrate that allows air flow to perturb the oil and aqueous volumes near the surface.

Lastly, in the case where no bilayer separates the aqueous volumes, conduction between the Ag/AgCl electrodes is dominated by the conductivity of the salt solution within each volume. The much lower electrical resistance to current flow in this case causes the baseline current to be much larger, such that vibrations of the hair do not produce a discernible increase in the background ion current in the system (not shown).

The power spectral density (PSD) of the temporal response also changes as a result of air flow across the hair cell system. Fig. 4 shows that when no air flow is applied, and the hair is not vibrating, the dominant frequency in the measured current is a 60 Hz component attributed to unshielded electrical interference (black trace). However, when the flow of air causes the hair to vibrate, two new frequency peaks appear at 225 Hz and 1589 Hz, respectively, in the power spectral content of the measured signal (red trace). Additionally, we observe that the same peak due to noise at 60 Hz again appears in the PSD of the measured current across the bilayer when air flow is present.

Phenomenologically, the response of the membrane-based artificial hair cell demonstrates that the motion of a hair translates into an increase in current measured across the lipid bilayer membrane. Similar to the cilia found in living hair cells, the artificial hair likely acts as mechanical lever, directing the force of the applied air pressure to the bilayer formed on the surface of

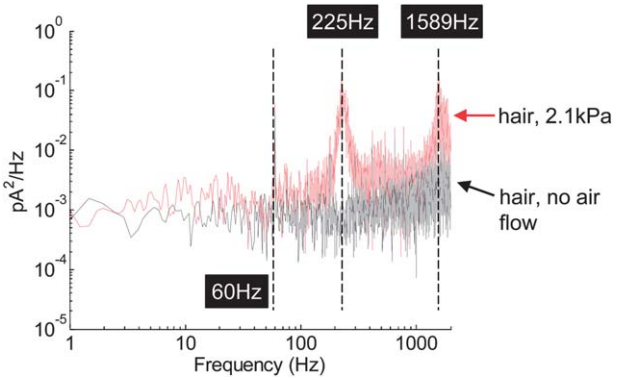

Fig. 4 Power spectral density, computed using Welch's method, of the hair cell system with (red trace) and without (black trace) air flow present.

the gel at the base of the hair. Furthermore, the results show that both the amplitude of the signal and the frequency content of the current are affected by the applied air flow across the hair. In the following sections, we present experimental data and discussions to elucidate the physics of this transduction mechanism and we investigate the influences of several parameters on the measured current from the biologically-derived air flow sensor, including: applied flow velocity (pressure), length of the hair, and the transmembrane potential. Furthermore, we will show that the mechanical vibrations of the hair are directly related to the frequency content of the measured current.

3.2 Physical mechanism for current generation

The structure of the lipid membrane that connects the two conductive aqueous media plays an important role in its physical response to electrical and mechanical stimuli. Geometrically, a bilayer consists of two leaflets of amphiphilic phospholipid monolayers organized such that the hydrocarbon tail side of each monolayer orients inwards, leaving the hydrophilic headgroups exposed to the water on each side of the membrane. This stable, yet highly fluid, organization of molecules is a favorable configuration that forms spontaneously (denoted by a decrease in free energy[25]) as excess oil is excluded from between the opposing lipid monolayers. The resulting lipid bilayer is represented electrically by a large resistance (>10 MΩ cm^2) in parallel with a capacitance (0.1–1.0 μF cm^{-2}),[29–31] where the nominal value of each term is a function of the membrane area.

In order to develop explanations for the measured current response of this system, we first note that air flow-induced motion of the hair creates a current response at frequencies well above 10 Hz (see Fig. 4). Given this observation and knowing that the equivalent impedance of a bilayer at frequencies between approximately 1 Hz and 10 kHz is described accurately by the capacitance of the membrane alone,[30,31] the following analysis treats the bilayer interface simply as a single capacitor.

Recalling that the charge developed across a capacitor is determined by the product of the capacitance, C, and the applied potential, V, and that charge is the integral of current, i, then the current that flows through a capacitor is written as

$$i(t) = \frac{d}{dt}(CV). \quad (1)$$

Expanding the time derivative in eqn (1) shows that both a time-varying potential or a time-varying capacitance generate current, as given by

$$i(t) = \frac{dC(t)}{dt} V(t) + \frac{dV(t)}{dt} C(t). \quad (2)$$

Eqn (2) suggests that the increase in current produced by a stream of air blown across the hair structure may be caused either by a time-varying capacitance, C, of the membrane or by a time-varying transmembrane potential, V. To differentiate which effects are present, we investigated each separately.

First, we measured the open circuit voltage across the bilayer during air flow for successive flows at exit pressures of 1.4 kPa (0.2 psi), 2.1 (0.3 psi), 2.8 (0.4 psi), and 3.4 kPa (0.5 psi) (not shown). When not regulated by an applied voltage, the transmembrane potential varied between −150 mV and −100 mV. We attributed this non-zero potential to the fact that during photopolymerization of the gel, some of the water evaporates, leaving a higher concentration of salt on the gel ((−)electrode) side of the bilayer. The measured transmembrane potential exhibited a small amount of drift as well, likely as double layers formed on the surface of the electrodes during the measurement, however no correlation was measured between the variation in potential and the application of air flow to the hair. PSD analysis of the open circuit voltage also confirmed that the frequency content of the signal (even during times of applied air flow) consisted of frequencies less than 10 Hz, with no distinct frequency peaks near 225 Hz or 1590 Hz as was observed in the PSD of the current trace. This result suggests that the voltage across the membrane is not correlated to the motion of the hair. Equally, however, the result indicates that presence of a transmembrane potential (even when not directly applied *via* the electrodes) may contribute to the measured signal as in the result shown in Fig. 3a.

Next, we investigated the possibility that temporal variation in the membrane capacitance is the dominant source of the current measured under an applied air flow. Based on a simplified version of eqn (2) that includes only the first product on the right hand side, we performed a second set of tests to determine if the capacitance of the membrane changes as a result of the vibrating hair, resulting in a current. In these tests, the current flowing through the membrane was measured for a fixed applied voltage while the hair was perturbed with steady air flow (2.1 kPa exit pressure). The applied potential was varied from 0–100 mV in 20 mV intervals and the amplitude of the measured currents, as well as the capacitance of the membrane measured prior to air flow tests, were recorded for each applied potential.

It is well established that the application of a constant potential across a bilayer will result in an increase in the capacitance of the membrane.[26,27,32] Fig. 5a shows that the capacitance of the bilayer increases from a value of 225 pF at 0 mV to more than 290 mV at |100 mV| (a 29% increase), following a linear trend with respect to V^2. This behavior—called *electrowetting* for solvent-containing lipid membranes—is explained by the Young–Lippmann equation,[26] which relates the contact angle of a liquid volume on a surface to both the surface tensions and the applied electric field. As the illustration in Fig. 5b shows, a decrease in the contact angle produces larger contact area between two volumes. This effect, along with a reduction in thickness of the bilayer due to electrocompression and redistribution of solvent remaining in the membrane, causes the capacitance of the interface to increase. Therefore, the capacitance of the bilayer can be written in terms of the applied voltage[33]

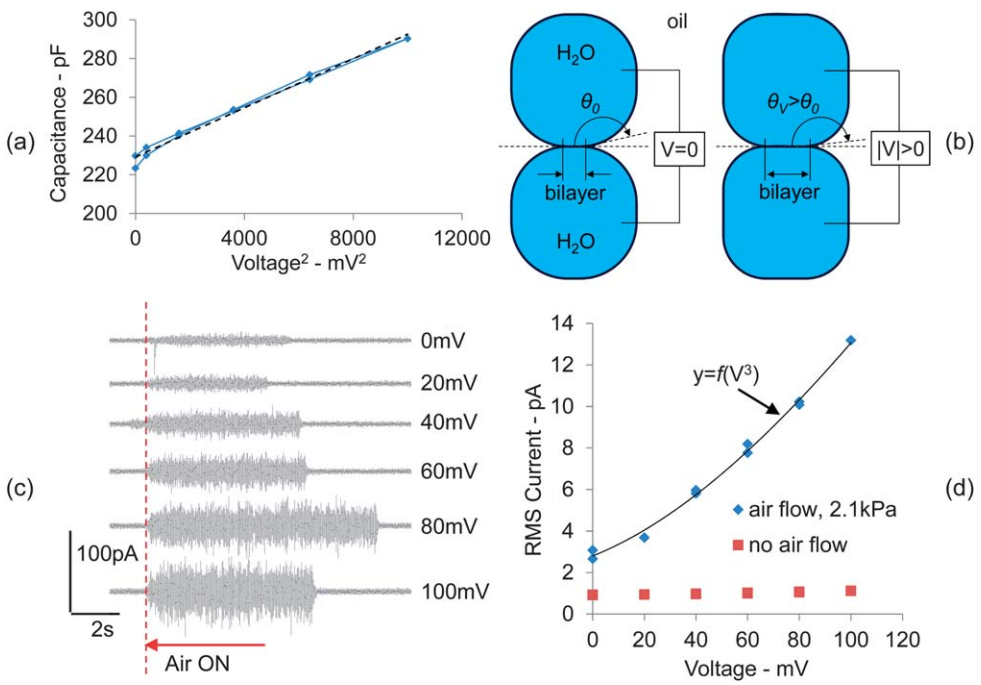

Fig. 5 (a) Capacitance measurements of the bilayer at potentials from 0–100 mV. (b) The applied voltage increases the size of the bilayer interface by reducing the contact angle between two lipid coated aqueous volumes. (c) Representative current traces at each potential show that the current during air flow increases in amplitude. (d). RMS current *versus* applied potential measured during air flow and under no flow conditions.

$$C(V, t) = C_0(t)(1 + \alpha V^2), \quad (3)$$

where, $C_0(t)$ is the capacitance at zero volts and α describes the voltage-dependence for a given membrane system. The variable of time, t, is included in the capacitive terms of this expression since we suspect that the membrane capacitance may change during excitation of the hair. A linear fit of the data in Fig. 5a produces estimates of 229 pF and 26 V^{-2} for C_0 and α, respectively. This estimate for α measured for DPhPC membranes formed in hexadecane is in good agreement with a value of 22 V^{-2} measured for suspended glycerol monooleate (GMO)/hexadecane membranes formed by White and Change.[32] In fact, the work by White and Chang[32] demonstrated that the amount to which a bilayer can increase in size due to voltage-induced solvent exclusion depends on the relative width of the annulus of excess oil that surrounds the bilayer. Smaller annuli restrict growth, while large annuli allow for much larger increases in size. Consequently, our estimate of α, which is larger than most values reported in the literature,[34–36] can be explained by the lack of a substrate (and the effectively large annulus of oil that surrounds the aqueous volumes) that allows for substantial increases in bilayer size.

Given the voltage dependent behavior of the membrane, eqn (2) and (3) can be used to develop an expression for the current generated by a change of capacitance at a constant applied voltage, V. First, the time derivative of eqn (3) for a constant voltage is determined using the product rule and is written as

$$\frac{dC(V,t)}{dt} = \frac{dC_0(t)}{dt}\left[1 + \alpha V^2\right]. \quad (4)$$

Substituting this expression into eqn (2), the current generated by a change in capacitance at constant potential can be written as

$$i(t) = \frac{dC_0(t)}{dt}\left[V + \alpha V^3\right]. \quad (5)$$

The current traces in Fig. 5c confirm that the current measured during air flow increases with the applied voltage. Moreover, the relationship between the amplitude of the current and the applied voltage (Fig. 5d) is not linear since both the capacitance (eqn (3)) and the time derivative of the capacitance (eqn (4)) are functions of voltage. Instead, the amplitude of the current increases with respect to the third power of voltage. Values for the coefficients of eqn (5), given by $\alpha\frac{dC_0(t)}{dt}$ and $\frac{dC_0(t)}{dt}$ for the third- and first-order coefficients, are estimated to be 1.186×10^{-6} nF s^{-1} mV^{-2} and 49.7 pF s^{-1}, respectively, using a third-order least squares fit of the data shown in Fig. 5d. The third-order coefficient is then divided by the experimentally-determined value of α (26 V^{-2}) in order to obtain a second estimate of 46.0 pF s^{-1} for $\frac{dC_0(t)}{dt}$. The consistency between these two estimates of the time rate of change of the capacitance suggests a close agreement between the predicted behavior and the measured current at different voltages.

However, if the capacitance of the membrane can be kept constant across all voltage levels (*i.e.* $\alpha = 0$), as given by

$$C(V, t) = C_0(t), \quad (6)$$

then, the current produced by a time-varying capacitance becomes a linear function of the applied voltage:

$$i(t) = \frac{dC_0(t)}{dt}V. \quad (7)$$

The regulated attachment method (RAM),[23,24] developed by Sarles and Leo, provides a unique capability for resizing (reducing and increasing) the area of contact between the aqueous volume and the hydrogel that holds the hair by controlling a mechanical force applied to the flexible supporting substrate. Since non-zero voltages increase membrane size, the applied force can be increased for each prescribed voltage level in order to reverse the added area of the bilayer caused by electrowetting. Repeating the measurements shown in Fig. 5, we performed a new set of tests in which the membrane capacitance was rebalanced with the RAM to its zero voltage value, C_0, after applying the voltage for each air flow measurement (Fig. 6a). The amplitudes of the current measured during air flow for all voltage levels are plotted in Fig. 6b and compared to the results obtained when the bilayer capacitance was not held constant.

The data shown in Fig. 6b are an important result in this study. By maintaining a constant average capacitance with respect to potential ($C(V) = C_0$) *via* the RAM, the amplitude of the current increases linearly with voltage as predicted by eqn (7). A linear least squares fit of these data indicates that the capacitance changes at a rate (the slope of the regression) of approximately 59 pF s^{-1} (RMS) for steady air flow regulated at an exit pressure of 2.1 kPa. In addition, the increase in current measured at zero volts (the intercept of the regression) is attributed to slight differences in the actual transmembrane potential *versus* the potential applied at the electrodes. A value of 59 pF s^{-1} for dC_0/dt also agrees well with values of 46–50 pF s^{-1} obtained from the current-*versus*-voltage measurements on the same hair cell

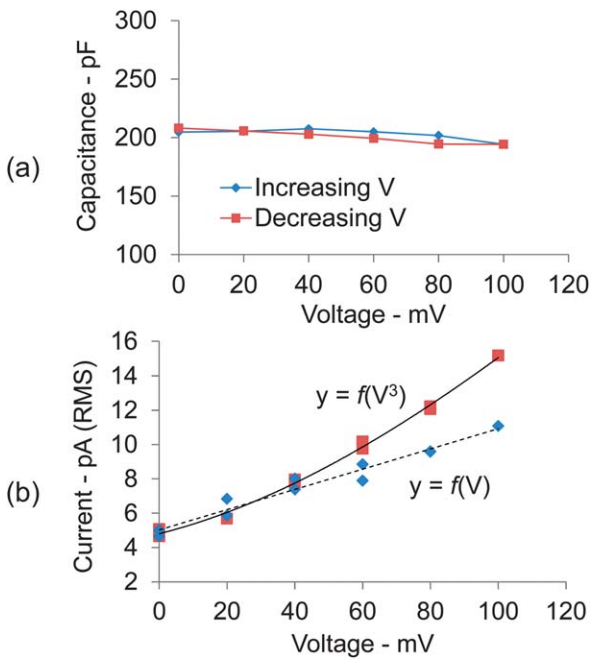

Fig. 6 (a) The RAM is used to maintain a constant capacitance at each potential level. (b) RMS current *versus* applied potential during air flow for a constant membrane capacitance (diamonds) are compared to RMS current measured for a voltage-dependent membrane capacitance (squares).

system in which the capacitance of the membrane was allowed to vary with voltage. And despite some variability in the size of the aqueous volumes and bilayers used to fabricate hair cells in this study, the effect of prescribing a constant membrane capacitance on the measured current is a repeatable phenomenon. This test was conducted two more times on different hair cells (same length of hair, new bilayers) and similar values, 47 pF s^{-1} (RMS) and 100 pF s^{-1} (RMS), respectively, for the time rate of change of capacitance were obtained for similar air flow conditions. Together, the data obtained from both approaches at quantifying the measured current for varying voltage levels provide strong evidence that a time-varying membrane capacitance is the cause the measured current.

We utilize the results of this analysis to estimate the dimensional change in the membrane area that is induced by the application of air flow to the sensor. Assuming that the capacitance of the membrane, $C(t)$, is represented as a sinusoidal waveform given by

$$C(t) = |C|\sin(\omega t), \tag{8}$$

we can also estimate the amplitude of the change of capacitance, $|C|$, from the measured RMS value for the time rate of change of the capacitance and the frequency, ω. By taking the derivative of eqn (8) and setting the RMS value of the amplitude equal to the measured value of dC/dt (RMS), we obtain the following expression

$$|C| = \frac{\sqrt{2}}{\omega}\left(\frac{dC}{dt}\right)_{RMS} \tag{9}$$

where, ω is the driving frequency in radians/s. For simplicity, assuming that the majority of the motion occurs at the first dominant frequency peak for the hair/bilayer system used in this set of measurements (250 Hz), a rate of capacitance change of 59 pF s^{-1} corresponds to a maximum change of only 0.053 pF, or 0.027% of the regulated membrane capacitance (200 pF, Fig. 6a).

While these results indicate that the capacitance of the bilayer oscillates when an air flow perturbs the hair, these data alone do not directly reveal exactly in what manner this time-varying capacitance occurs. Is the bilayer increasing in area at a constant thickness (*i.e.* is there free exchange of lipids at the edges of the bilayer)? Is the membrane stretching? Is the membrane bending?

In order to better understand the relationship between motion of the hair and the induced current signal, we also collected simultaneous high speed video of a 12 mm long hair and measurements of current across the membrane. The respective frame rate and sampling rate were both set to 2 kHz and the measurements were synchronized in time. The data plotted in Fig. 7a show two traces: the top trace is the measured current while the bottom trace is the motion of the tip of the hair. The data show that the hair exhibits both a dc change in position due to the mean flow and an oscillatory response. However, the static position of the hair does not contribute to the measured current, and as a result, the increase in the measured current lags the initial change in position that occurs at the 3 s mark.

The PSD of each signal is computed for the measured data for the time period between 4 and 7 s (Fig. 7b). Major peaks in both signals are observed at frequencies of approximately 190 and 320 Hz, respectively, while the PSD of the measured current also

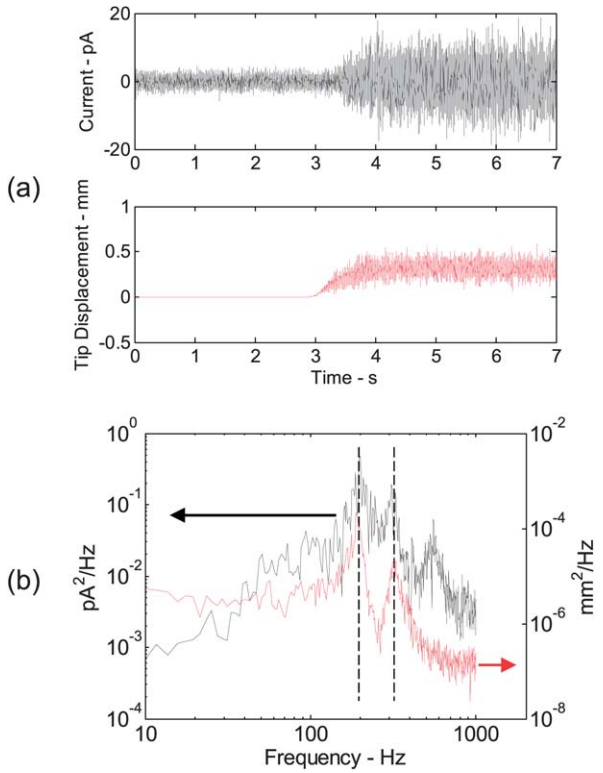

Fig. 7 (a) Synchronized current (top trace) and hair displacement (bottom) measurements are obtained using a single trigger to initialize high speed video capture and current recordings. (b) The PSD of each signal during air flow ($4 < t < 7$ s) is computed in order to compare the frequency content of the motion of the hair and the measured current through the bilayer.

displays a third, smaller peak at 550 Hz. The similar frequency spectra of both data indicate that changes in capacitance of the membrane are correlated to the motion of the hair. The third peak at 550 Hz for the measured current is likely caused by motion of the oil phase that surrounds base of the hair cell.

The frequency analysis of these synchronized signals provides important information in determining the physical mechanism for this change in membrane capacitance. Three possible structural modifications of the membrane that could generate a change in the electrical capacitance include: a change in the area of the interface at constant thickness, a change in the curvature of the membrane, or in-plane stretching (and thinning) of the bilayer. Due to the fact that dominant hair vibrations and current fluctuations are well above 100Hz for the 12 mm hair, then the capacitance changes too quickly for the free exchange of lipids to produce changes in the area of the bilayer, a phenomenon that occurs at frequencies less than 1 Hz.[18] Instead, the range of the frequency content of the measured current suggests that the membrane either bends or stretches.

Based on the work by Petrov *et al.*, to examine the flexoelectric effect of liquid crystal membranes such as lipid bilayers,[18,19,21] curvature induced changes in the membrane occur at the same frequency as either the mechanical or electrical input to the bilayer, while membrane stretching (and thinning) occurs at twice the driving frequency. Since our data also indicate that the current response is directly correlated with the frequency of hair

vibration, and not twice the frequency, we believe that membrane bending is the cause for the current produced as a result of air flow. This conclusion is further supported by the fact that the expansion elasticity of bilayers is much higher than the curvature elasticity (6×10^{-10} J *versus* 10^{-20} J, respectively[19,37]). Thus, less force is required to cause bending than induce planar stretching of the interface. We note that because the applied voltages are relatively small and because neutral (zwitterionic) phospholipids were used, the polarization of the membrane due to air-flow induced curvature (flexoelectric effect) may be limited[20,38] and an increased electrical response could possibly be obtained by maximizing the polarizability of the bilayer.

3.3 Dependence on flow rate and hair dimensions

Finally, we examined the sensitivity that the hair cell system exhibits in response to varying applied flows and hair dimensions.

Fig. 8a presents a plot of the measured current *versus* applied air pressure on hairs of varying lengths. In general, as the hair gets longer and the speed of the flow increases, the magnitude of the current grows. However, the measured current for the shortest hair tested (~3 mm) is not much larger than when air flows across the system without a hair, since a portion of the hair length is still surrounded by oil held in the substrate.

The sensitivity for each hair length is determined by taking the slope of the current *versus* air pressure data. The second plot in Fig. 8b shows that hair lengths of 6–12 mm have higher sensitivity (~3 pA(RMS) kPa^{-1}), however there is some variability in the sensor output as indicated by the range of measured slopes given by the error bars. The variation in sensitivity for hair cells of different lengths is likely due to differences in how each gel supports the hair and how the substrate constrains the gel, as well as slight differences in hair geometry and stiffness. These data may also suggest that there is a trade off between hair flexibility and stiffness in converting air flow into vibrations at the bilayer membrane.

A change in the length of the hair also affects the frequency content of the measured current. Fig. 9 shows that the first resonance frequency obtained from PSD of current measurements on four different length hairs decreases with increasing length.

For comparison, the first resonance frequencies of a cylindrical cantilevered hair[39] of varying length are simulated using measured values of 1.3 g cm^{-3} and 8.5 GPa, respectively, for the mass density and elastic modulus of the hairs used in this study. The lower resonance frequencies measured for the artificial hair cells indicate a difference in the boundary conditions between the hairs supported by a gel and a true cantilevered hair. Specifically, the fact that the resonance frequencies of the hair are lower than that of a cantilever beam (by a factor of approximately 1.6) suggest that the base of the hair may be able to rotate slightly in the gel during flow-induced vibration. A difference in boundary conditions does not affect the dependence of the resonance frequency on hair length; the measured resonance frequencies for gel-supported hairs, like a cantilevered hair, are inversely proportional to the square of the length.[39]

Despite the observed variability in the sensitivities of the hair cells studied in this initial work, the data in Fig. 8 and 9 provide additional confirmation that motion of the hair, which is prescribed by both the geometry and material properties of the hair and gel and also the applied air flow, creates changes in membrane geometry that induce current flow. Furthermore, this relationship suggests that higher-order resonance peaks seen in the PSDs of current traces are likely due to higher-order mechanical vibration modes of the hair.

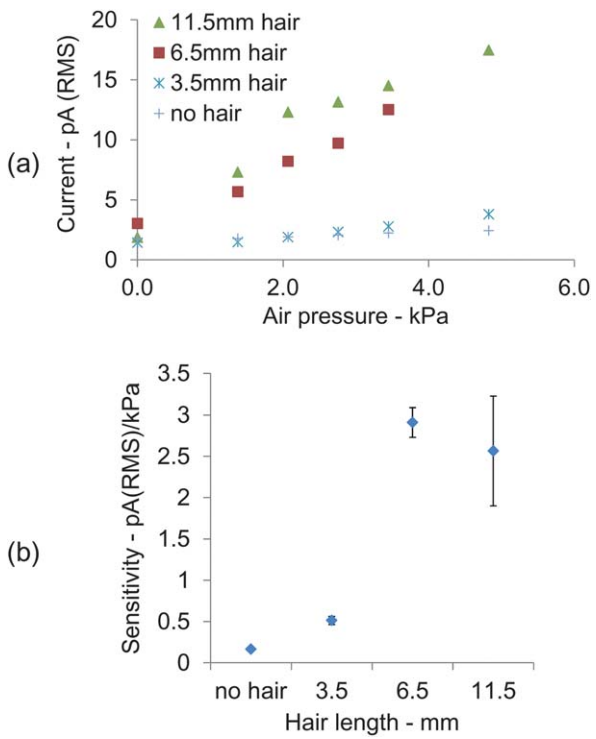

Fig. 8 (a) RMS current *versus* air flow exit pressure are compared for hairs of different lengths. (b) The sensitivity of the hair cell, defined as the slope of the measured RMS current *versus* flow pressure, for each hair length.

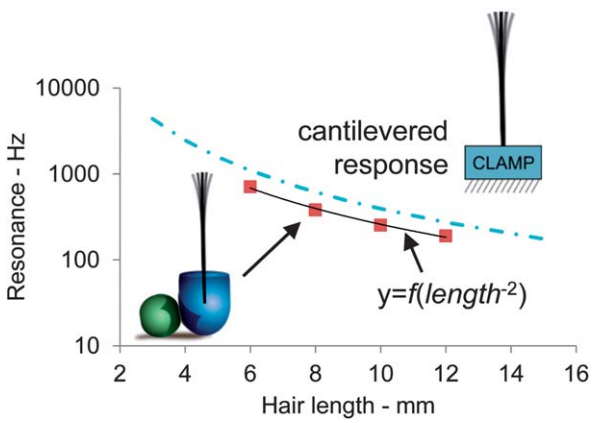

Fig. 9 The first resonance frequencies of the measured current signals for the artificial hair cells are plotted *versus* hair length and compared to simulated resonance frequencies for a cylindrical, cantilevered beam of varying length. The following parameters were used to compute the predicted resonance frequencies of a cantilevered hair: hair diameter = 110 μm, mass density = 1.3 g cm^{-3}, and elastic modulus = 8.5 GPa, respectively.

3.4 Comparison to natural hair cells

In context to these results, we feel it is important to briefly address some fundamental differences between living hair cells and our artificial hair cell sensor. Our synthetic device mimics the basic function of hair cells in that bending of a cilia-like structure induces an electrical response at a cellular interface. The specific transduction mechanism was found to be a vibration-induced change in capacitance of the artificial lipid bilayer that results in an increased current across the membrane. In contrast, the transduction mechanism used by both mammalian inner and outer hair cells is performed *via* mechanically-activated ion channels located in bilayer membranes that encase the stereocilia. As the cilia bend, the opening of ion channels result in an inward cation flux that depolarizes the cell interior.[15,40] Despite these differences in transduction, the fact that the artificial bilayer formed in our system is comprised of phospholipids allows for this interface to host other biological molecules, including ion channels, to possibly alter or enhance transduction in ways similar to natural hair cells.

The difference in transduction mechanism also affects the length scale of operation for each system. Living hair cells, which are typically less than 100 μm in total length,[6] are responsive to displacements of the cilia on the order of only 1 nm since the gating of ion channels occurs on a molecular scale.[40] The initial sensor studied in this work was not only much larger (mm-scale) but required larger motions of the synthetic hair in order to induce an electrical response. Nonetheless, we believe that our system can be assembled on much smaller length scales (~1 μm), whereby both the size of the hair cell system and the minimum required motion of the cilia to induce a measurable response can approach that of living hair cells.

4 Conclusions

The membrane-based artificial hair cell system presented in this paper offers a new approach for building mechanoelectric sensors, one that is inspired by the structure and function of mammalian hair cells. The key property of our system is the mechanoelectrical response of a lipid bilayer membrane formed at the surface of the gel used to support the hair. Our data indicate that the motion of a synthetic hair due to an applied air flow is directly correlated to the magnitude and frequency content of the measured current across the bilayer. The physics of this transduction mechanism were investigated through a series of experiments in which the voltage across the bilayer was varied. Our investigations support the hypothesis that the current induced by motion of the hair cell is related to the change in capacitance caused by motion of the bilayer membrane. Analysis of the capacitance variation leads us to believe that the dimensional changes in the bilayer membrane are less than 1 part in 1000, which is consistent with the belief that membrane bending is the cause of the capacitance variation. This conclusion is also supported by the fact that the frequency of oscillation of the current response is directly correlated with the bending frequency of the hair. Thus, we believe that motion of the hair induces bending of the lipid bilayer membrane and results in the generation of a current response across the bilayer. Futhermore, our results demonstrate that the amplitude of the measured current scales proportionally with the transmembrane voltage, the flow rate of air, and the length of the hair. Hair cells constructed using artificial hairs with lengths from 3–12 mm exhibited sensitivities in the range 0.5–3.5 pA(RMS) kPa^{-1}, with first resonance frequencies occurring within the range 0.1–1.0 kHz as a result of the applied air flow.

Acknowledgements

The authors gratefully acknowledge financial support from the National Science Foundation (EFRI-0938043) and the Office of Naval Research (N000140810654).

References

1 S. P. Sane and M. J. McHenry, *Sensory Biomechanics, Integrative and Comparative Biology*, Boston, MA, 2009.
2 M. McHenry, J. Strother and S. van Netten, *J. Comp. Physiol., A*, 2008, **194**, 795–810.
3 F. G. Barth, *Naturwissenschaften*, 2000, **87**, 51–58.
4 Albert, Friedrich, Dechant and Barth, *J. Comp. Physiol., A*, 2001, **187**, 303–312.
5 P. Dallos and B. N. Evans, *Science*, 1995, **267**, 2006–2009.
6 R. M. Raphael, A. S. Popel and W. E. Brownell, *Biophys. J.*, 2000, **78**, 2844–2862.
7 J. M. Engel, J. Chen, L. Chang and D. Bullen, *J. Microelectromech. Syst.*, 2006, **15**, 729–736.
8 C. Liu, *Bioinspir. Biomimetics*, 2007, **2**, S162.
9 S. Peleshanko, M. D. Julian, M. Ornatska, M. E. McConney, M. C. LeMieux, N. Chen, C. Tucker, Y. Yang, C. Liu, J. A. C. Humphrey and V. V. Tsukruk, *Adv. Mater.*, 2007, **19**, 2903–2909.
10 M. E. McConney, N. Chen, D. Lu, H. A. Hu, S. Coombs, C. Liu and V. V. Tsukruk, *Soft Matter*, 2009, **5**, 292–295.
11 P. R. Downey and A. B. Flatau, *J. Appl. Phys.*, 2005, **97**, 10R505.
12 P. D. McGary, L. Tan, J. Zou, B. J. H. Stadler, P. R. Downey and A. B. Flatau, *J. Appl. Phys.*, 2006, **99**, 08B310.
13 P. R. Downey, A. B. Flatau, P. D. McGary and B. J. H. Stadler, *J. Appl. Phys.*, 2008, **103**, 07D305.
14 J. J. Park, M. Reddy, C. Mudivarthi, P. R. Downey, B. J. H. Stadler and A. B. Flatau, *J. Appl. Phys.*, 2010, **107**, 09A954.
15 F. Sachs, W. Brownell and A. Petrov, *MRS Bull.*, 2009, **34**, 665–670.
16 P. Dallos and B. Fakler, *Nat. Rev. Mol. Cell Biol.*, 2002, **3**, 104–111.
17 J. Zheng, W. Shen, D. Z. Z. He, K. B. Long, L. D. Madison and P. Dallos, *Nature*, 2000, **405**, 149–155.
18 A. G. Petrov and V. S. Sokolov, *Eur. Biophys. J.*, 1986, **13**, 139–155.
19 A. T. Todorov, A. G. Petrov and J. H. Fendler, *J. Phys. Chem.*, 1994, **98**, 3076–3079.
20 A. T. Todorov, A. G. Petrov and J. H. Fendler, *Langmuir*, 1994, **10**, 2344–2350.
21 A. G. Petrov, *Anal. Chim. Acta*, 2006, **568**, 70–83.
22 S. A. Sarles and D. J. Leo, *Lab Chip*, 2010, **10**, 710–717.
23 S. A. Sarles and D. J. Leo, *Anal. Chem.*, 2010, **82**, 959–966.
24 S. A. Sarles, L. J. Stiltner, C. B. Williams and D. J. Leo, *ACS Appl. Mater. Interfaces*, 2010, **2**, 3654–3663.
25 D. Needham and D. A. Haydon, *Biophys. J.*, 1983, **41**, 251–257.
26 J. Requena and D. A. Haydon, *J. Colloid Interface Sci.*, 1975, **51**, 315–327.
27 S. Punnamaraju and A. J. Steckl, *Langmuir*, 2010, **27**, 618–626.
28 M. A. Holden, D. Needham and H. Bayley, *J. Am. Chem. Soc.*, 2007, **129**, 8650–8655.
29 H. T. Tien and A. L. Ottova, *J. Membr. Sci.*, 2001, **189**, 83–117.
30 W. Romer and C. Steinem, *Biophys. J.*, 2004, **86**, 955–965.
31 S. A. Sarles and D. J. Leo, *J. Intell. Mater. Syst. Struct.*, 2009, **20**, 1233–1247.
32 S. H. White and W. Chang, *Biophys. J.*, 1981, **36**, 449–453.

33 O. Alvarez and R. Latorre, *Biophys. J.*, 1978, **21**, 1–17.
34 D. Rosen and A. M. Sutton, *Biochim. Biophys. Acta, Biomembr.*, 1968, **163**, 226–233.
35 S. H. White and T. E. Thompson, *Biochim. Biophys. Acta, Biomembr.*, 1973, **323**, 7–22.
36 S. H. White, *Biophys. J.*, 1978, **23**, 337–347.
37 E. Evans and W. Rawicz, *Phys. Rev. Lett.*, 1990, **64**, 2094.
38 B. Harland, W. E. Brownell, A. A. Spector and S. X. Sun, *Physical Review E*, 2010, **81**, 031907.
39 D. J. Inman, *Engineering Vibration*, Prentice-Hall, Inc., Upper Saddle River, New Jersey, 2nd edn, 2001.
40 A. J. Hudspeth, *Nature*, 1989, **341**, 397–404.